ACS APPLIED MATERIALS & INTERFACES

www.acsami.org

Research Article

Photocrosslinkable Polymeric Bicontinuous Microemulsions

Michael B. Sims, Joshua W. Goetze, Gabriela Diaz Gorbea, Zachary M. Gdowski, Timothy P. Lodge,* and Frank S. Bates*

Cite This: *ACS Appl. Mater. Interfaces* 2023, 15, 10044−10052

Read Online

ACCESS | Metrics & More | Article Recommendations | Supporting Information

ABSTRACT: We present an approach to photocrosslink bicontinuous microemulsions derived from ternary blends of poly(methoxyethyl acrylate) (PM, M_n = 4200 g/mol), poly(hexyl methacrylate-*co*-coumarin methacrylate) (PHC, M_n = 6800 g/mol), and PM-*b*-PHC diblock polymer (M_n = 19,400 g/mol) in a phase-selective manner, enabling structural characterization at an unprecedented level of detail. This strategy utilizes the [2 + 2] photodimerization reaction of coumarin derivatives to covalently crosslink blends without the use of harsh reagents or disruptive thermal treatment, thus preserving the intricate network structure throughout curing. The resulting crosslinked bicontinuous microemulsions exhibited rubbery behavior at elevated temperatures, achieving an elastic shear modulus of nearly 1 MPa at 70 °C, owing to the presence of the three-dimensional co-continuous network morphology. The dimensional stabilization afforded by crosslinking further allowed the microstructure to be directly imaged by scanning electron microscopy and atomic force microscopy. Contrary to recent theoretical findings, the BμE appears in a wide temperature and compositional window, suggesting that it is a robust feature of these blends. As a proof of concept demonstrating both the utility of bicontinuous microemulsion-derived materials and versatility of this strategy toward broader applications in energy storage and transport, the uncrosslinked portion of a cured blend was extracted by washing and replaced with an ionic liquid; the resultant heterogeneous solid electrolyte exhibited a room-temperature conductivity of 2 mS/cm, approximately one-quarter that of the pure ionic liquid.

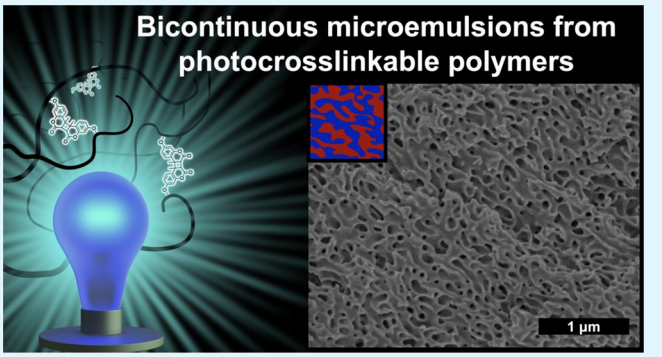

KEYWORDS: *bicontinuous microemulsion, nanoporous materials, polymer blends, coumarin, photocrosslinking, diblock polymers, microphase separation*

INTRODUCTION

As increasingly complex societal challenges demand increasingly sophisticated materials design, co-continuous networks have emerged as a highly adaptable class of nanostructured polymers.[1−3] Featuring independent, structured, and fully percolating domains of different polymers, co-continuous network morphologies enable disparate and even contradictory properties to be engineered within a single material.[4] As the network domain size is governed by the molecular weight of the constituent (macro)molecules, these mesophases also have substantial utility as templates for nanoporous materials.[5−11] In 1997, Bates and colleagues discovered that certain ternary blends of A and B homopolymers and a compatibilizing AB diblock polymer formed a bicontinuous microemulsion (BμE),[12] a co-continuous network phase historically encountered in water/oil/surfactant emulsions[13] but previously unreported in polymer materials. The BμE is a rare example of a (meta)stable network phase that generally requires no special synthesis or processing beyond blending of the constituent polymers. In contrast, many other co-continuous network materials require specialized preparation due to their thermodynamic instability toward macrophase separation — and an accompanying destruction of advantageous properties.[14−18]

Since its initial discovery, the BμE has been found in a multitude of chemically and compositionally diverse polymer blends,[19−34] pointing to it being a universal phase in soft matter. However, recent theoretical findings by Matsen and colleagues have questioned its existence at equilibrium in polymer blends. Based on field-theoretic simulations, they posit that BμE does not exist as a pure phase, instead existing only as one component of a macroscopically separated three-phase coexistence (A-rich, B-rich, and BμE) within a narrow temperature and compositional window.[35,36] Considering that most BμEs are largely characterized by small-angle X-ray and/or neutron scattering, with direct images of the morphology

Received: December 21, 2022
Accepted: January 30, 2023
Published: February 12, 2023

https://doi.org/10.1021/acsami.2c22927
ACS Appl. Mater. Interfaces 2023, 15, 10044−10052

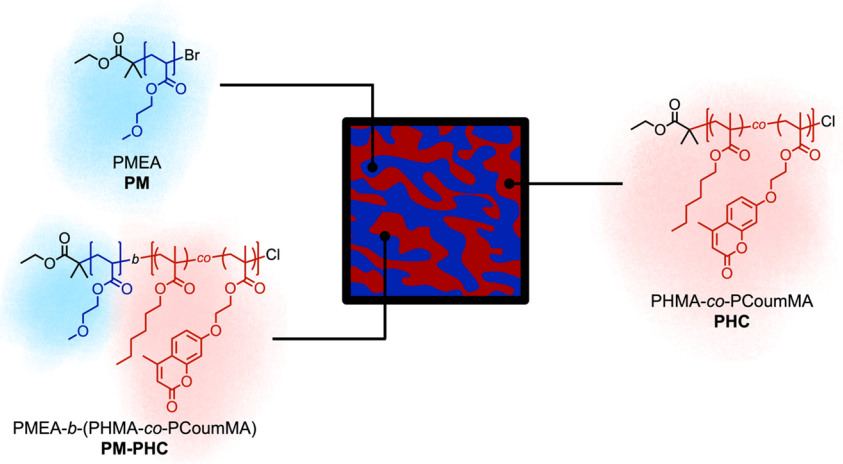

Figure 1. Schematic depiction of the BμE morphology and corresponding polymers that comprise each phase and interface in this photocrosslinkable system.

seldom captured, more definitive characterization is needed to validate this morphology for end-use technologies. Additionally, the narrow window of phase space in which the BμE appears presents a substantial restriction to characterization and application strategies. Crosslinking the morphology would impart increased thermal/chemical stability and broaden the range of environmental/processing conditions to which it can be safely employed in industrially relevant applications. A previously reported BμE crosslinking approach, involving vulcanization of polyisoprene domains with S_2Cl_2,[37] is not suitable for addressing these issues, as the harsh reagents can swell the delicate morphology; it also proved difficult to regulate the degree of crosslinking. A more controllable and less destructive method for covalent crosslinking is therefore needed.

In this work, we develop a new approach to crosslink polymeric BμEs using coumarin [2 + 2] photodimerization. This reaction is mediated by long-wavelength UV light[38] and has been utilized in solution-based polymeric systems,[39−45] polymer melts,[46−48] and microphase-separated diblock polymers.[49,50] Importantly, the ability to perform coumarin-based photocrosslinking without exogenous reagents or thermal treatment ensures that the microstructure will be minimally perturbed during curing. In the ternary blends studied herein, we find that coumarin photodimerization can crosslink and covalently stabilize emergent morphologies, including the BμE, with minimal disruption to the microscopic structure. Consequently, we were able to directly image the BμE structure with unprecedented resolution using scanning electron microscopy and atomic force microscopy. These images definitively validate the previously hypothesized structure of the BμE as a fluctuating co-continuous structure, and at appropriate compositions, no evidence is found of widespread macrophase separation. We additionally found that in this system, the BμE exists in a nearly pure state or in coexistence with lamellae over a range of 78−86 vol % homopolymer, a significantly wider window in neutral blends than anticipated from previous X-ray/neutron scattering data. The emergent physical properties were studied through in situ photorheometry, where the strong increase in modulus upon curing was recorded for microphase separated blends, including those featuring BμE structures. As a final demonstration of application, a crosslinked blend was prepared in which one of the co-continuous phases was replaced with a conductive ionic liquid, and the resultant solid polymer electrolyte exhibited a room temperature conductivity of 2.0 mS/cm—a value approximately one quarter of that characterizing the pure ionic liquid.

RESULTS AND DISCUSSION

Material Design and Characterization. Photocrosslinkable A/B/AB ternary blends were designed around the polymer chemistries utilized in a previous report,[49] consisting of a poly(methoxyethyl acrylate) (PM) homopolymer, a crosslinkable poly(hexyl methacrylate-*co*-coumarin methacrylate) (PHC) statistical copolymer, and a compatibilizing diblock polymer PM-PHC (Figure 1). The polar PM polymers are sufficiently incompatible with the nonpolar PHC polymers that (micro)phase separation occurs at accessible temperatures, even with relatively low-molecular-weight species. The use of polymers with low glass transition temperatures (T_g) further facilitates crosslinking, as the inter-chain coumarin dimerization reaction cannot reach high conversion without chain mobility; low coumarin reactivity has been observed when the photocrosslinking reaction is conducted below the bulk T_g.[50] To determine the effect on the glass transition imparted by coumarin-bearing structural units, we synthesized three PHC statistical copolymers with coumarin methacrylate monomer mole fractions (x_{CoumMA}) spanning x_{CoumMA} = 0.09−0.28 and measured the respective T_gs with differential scanning calorimetry (Figure S1). From Flory−Fox analysis, an extrapolated value of T_g = 166 °C for the PCoumMA homopolymer was found (Figure S2). While reaction kinetics considerations anticipate that the photocrosslinking rate can be increased by increasing the amount of CoumMA, at a certain point this trend might be counteracted by the excessive glassiness of the polymer matrix. Vitrification in the vicinity of the order−disorder temperature will also suppress phase transitions, so we elected to target a moderate coumarin incorporation (x_{CoumMA} = 0.30) for subsequent blend materials, which exhibits a T_g of 44 °C compared to the known T_g of the poly(hexyl methacrylate) homopolymer of −5 °C.[51]

All polymers were synthesized by atom-transfer radical polymerization,[52,53] which enabled precise control over polymer compositions and molecular weights (Table 1). The absolute molecular weights of the ternary blend components

https://doi.org/10.1021/acsami.2c22927
ACS Appl. Mater. Interfaces 2023, 15, 10044−10052

Table 1. Molecular Characterization

polymer	$M_{n,SEC}$ (g mol^{-1})[a]	N[b]	$Đ$[a]	x_{CoumMA}[c]	f_{PHC}[d]
PM	4200	64	1.02		
PHC	6800	100	1.07	0.31	
PM-PHC	19,400	290	1.13	0.29	0.43

[a]Absolute molecular weight determined by size-exclusion chromatography with multi-angle light scattering. [b]Volumetric degree of polymerization calculated using a reference volume of 0.100 nm^3, literature densities for PM (ρ = 1.09 g/mL) and poly(hexyl methacrylate) (ρ = 1.01 g/mL), and estimated density of poly(coumarin methacrylate) density (ρ = 1.23 g/mL) from Van Krevelen's group contribution method.[55] [c]Determined by NMR spectroscopy. [d]Volume fraction of the crosslinkable PHC block.

affect the order−disorder transition temperatures (T_{ODT}) on the diblock polymer-rich side and the critical temperatures on the homopolymer-rich side and therefore were kept relatively low in our system in order to promote rapid ordering kinetics and achieve accessible order−disorder transitions (ODTs). Additionally, the molecular weight ratio of the homopolymer components to the diblock polymer (α) substantially influences the phase behavior of ternary blends[54] and is represented by the following expression:

$$\alpha = \frac{N_{H,av}}{N_{DB}} \quad (1)$$

where $N_{H,av}$ is the average volumetric degree of polymerization of the homopolymers and N_{DB} is the volumetric degree of polymerization of the diblock polymer; $N = M_n/(N_A \rho v)$ where M_n is the number average degree of polymerization, N_A is the Avogadro constant, ρ is the polymer density, and v is the reference volume (0.100 nm^3). As the mean-field Lifshitz point occurs only when $\alpha < 1$,[54] we targeted $\alpha = 0.28$ in this system, consistent with several previous studies.[19,21,24]

Phase Behavior of Ternary Blends. The full phase behavior of homopolymer/homopolymer/diblock polymer ternary blends is captured by a 4-parameter phase prism, where the relative compositions of the two homopolymers and the diblock polymer compose a ternary phase diagram and temperature is the vertical axis. To reduce this system to a manageable parameter space, theory and experiment typically focus on blend compositions with equivolumetric amounts of A and B structural units (i.e., $\phi_A = \phi_B = 0.50$). The 4-parameter phase prism then simplifies to a 2-parameter volumetrically symmetric isopleth, where the vertical axis is temperature and the horizontal axis is the combined A/B homopolymer volume fraction (ϕ_H) defined as

$$\phi_H = \phi_A + \phi_B = 1 - \phi_{AB} \quad (2)$$

The diblock polymer-rich side of the ternary blend phase diagram features a line of ODTs that marks the lamellae (LAM)−disorder phase boundary, while the homopolymer-rich side is defined by a Scott line of critical points that marks the multiphase−single-phase boundary. Where these two lines meet, self-consistent field theory predicts the existence of an isotropic Lifshitz point at which LAM, macroscopic multiphase, and one-phase disordered states coexist.[56] Theory further predicts that as lamellae are increasingly swollen with a homopolymer, the microphase-separated ordered state proceeds through a three-phase coexistence window of disordered A-rich, B-rich, and LAM phases which transitions to two macroscopic phases as $\phi_H \to 1$.[57] (The original mean-field theory predicted a lamellar unbinding transition that directly yielded two-phases as ϕ_H was increased).[58] Yet, the Lifshitz point is not actually observed in finite molecular weight polymer systems due to the intervention of composition fluctuations that breaks the second-order (critical) character of the LAM-DIS transition.[27,59] Instead, a BμE channel appears in place of the Lifshitz point, coincident with the bending modulus of the lamellar layers approaching kT, where k is Boltzmann's constant. Recent refinements of the theory associated with symmetric A/B/AB ternary blends lead to the conclusion that the BμE state does not extend to segregation strengths greater than that associated with the end of the line of LAM-DIS transitions with increasing ϕ_H; i.e., there is no BμE channel at lower temperatures.[35,36]

To explore this phase space in this crosslinkable system, PM/PHC/PM-PHC ternary polymer blends were prepared spanning a range of ϕ_H. Blends with compositions ϕ_H = 0.76−0.90 all exhibit some turbidity (Figure 2), although the marked

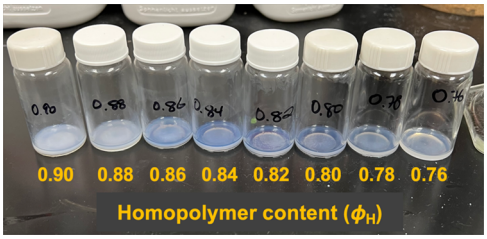

Figure 2. Blends prepared in the vicinity of the bicontinuous microemulsion channel.

increase in opacity of the ϕ_H = 0.88 and 0.90 blends implies the onset of macrophase separation. This change in appearance coincides with the location of the SCFT-predicted Lifshitz point at $\phi_{H,LP} = (1 + 2\alpha^2)^{-1} = 0.87$[54] that demarcates the boundary between micro- and macrophase separated regimes. The hazy blue color of blends with compositions $\phi_H \leq 0.86$ is attributed to light scattering by BμE domains (see below), as has been seen in oil/water/surfactant BμEs.[60]

Small-angle X-ray scattering (SAXS) was used to characterize both the morphology and approximate order−disorder transition temperatures (T_{ODT}) of uncrosslinked ternary blends as a function of ϕ_H (Figures 3 and S3). At 25 °C, LAM appears from ϕ_H = 0−0.76 as indicated by a strong peak at relatively high q values (while additional higher-order reflections are not evident, the presence of LAM is inferred from the volumetric symmetry of the blends). The morphology transitions to a BμE from ϕ_H = 0.78−0.90, as evident by the presence of a single broad maximum at low q. This peak weakly persists in the opaque blends (ϕ_H = 0.88−0.90), suggesting 3-phase coexistence between macrophase-separated PM-rich and PHC-rich domains and a BμE. At 85 and 115 °C, LAM/BμE coexistence appears from ϕ_H = 0.78−0.80 as indicated by the presence of a high-q shoulder on the BμE peak (e.g., the peak at q = 0.0118 Å^{-1} for ϕ_H = 0.80 in Figure 3), a feature that has also been observed in neutral[24] and partially charged[21] ternary blends.

The domain spacing (d) was extracted from the principal scattering peak (q^*) using the relation

$$d = \frac{2\pi}{q^*} \quad (3)$$

https://doi.org/10.1021/acsami.2c22927
ACS Appl. Mater. Interfaces 2023, 15, 10044−10052

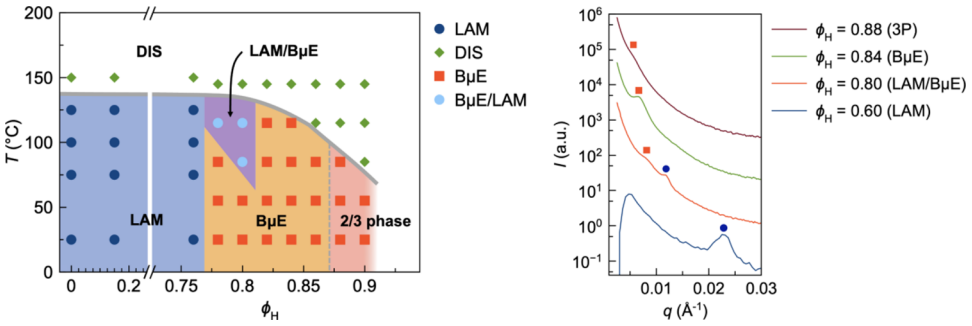

Figure 3. Volumetrically symmetric isopleth determined by SAXS and microscopy for PM, PHC, and PM-PHC blends where ϕ_H refers to the combined volume fraction of PM and PHC (left); SAXS patterns obtained at 75 °C (ϕ_H = 0.60) and 85 °C (ϕ_H = 0.80−0.88) for blends exhibiting LAM, LAM/BμE, BμE, and multiphase morphologies (right). Markers refer to phases observed in SAXS. LAM = lamellar; DIS = disordered; BμE = bicontinuous microemulsion. The label 2/3 phase refers to two (homopolymer rich) or three (BμE and homopolymer rich) phases.

and plotted as a function of ϕ_H in Figure 4. Two regimes are clearly visible: in the highly swollen region (ϕ_H = 0.76−0.90),

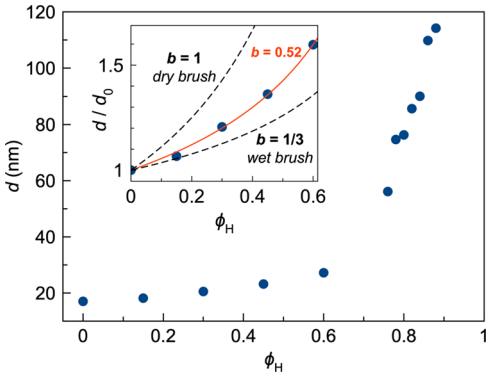

Figure 4. Evolution of domain spacing (d) at 25 °C as a function of combined homopolymer volume fraction (ϕ_H). The inset depicts domain spacing normalized to that of pure PM-PHC (d/d_0) with a fit to the equation $d/d_0 = (1 - \phi_H)^{-b}$, where the dashed lines represent the dry-brush limit (b = 1) and wet-brush limit (b = 1/3) of homopolymer swelling behavior.

d sharply increases as the composition approaches the Lifshitz point, which is a characteristic feature of BμE-forming ternary blends;[31,61] the maximum d achieved is over six times greater than the neat diblock polymer. In the pure-to-moderately swollen LAM region (ϕ_H = 0−0.60), the domain spacing scales with ϕ_H according to the power law relation $d/d_0 = (1 - \phi_H)^{-b}$, where the exponent b represents the ability of the homopolymer to swell the interfacial diblock polymer chains. Two limiting behaviors are dry-brush swelling (b = 1),[56] in which the lamellar copolymer brushes expel the homopolymer into the inter-lamellar space, and wet-brush swelling (b = 1/3),[62] where homopolymers infiltrate and swell the individual diblock chains. In this system, b = 0.52 was measured, which indicates partial wetting of the interfacial copolymer brush. We note that the molecular weight ratio of the PHC polymer to the PHC block in PM-PHC (0.79) is higher than that of the PM polymer to the PM block in PM-PHC (0.37), so the PHC domains likely undergo dry-brush swelling whereas the PM domains favor wet-brush swelling.

Direct Morphological Imaging via Microscopy. Typically, polymeric bicontinuous microemulsions have been characterized by fitting the scattering peak from small-angle X-ray or neutron scattering to the form factor described by Teubner and Strey[63] and then extracting metrics that quantify the domain spacing, inter-domain correlation length, and microemulsion structure.[64] To obtain meaningful data, this method requires the presence of a well-resolved microemulsion peak and careful background subtraction. Even so, details about both the local and global structure cannot be obtained by scattering pattern analysis alone. Given that crosslinking stabilizes microphase-separated polymer morphologies against thermal, mechanical, and chemical disruption, we reasoned that our cured blends would be well-suited for imaging in order to accurately assess the bulk microstructure.

Polymer blends spanning a compositional range of ϕ_H = 0.60−0.88 were photocured for 10 h at 70 °C with a 365 nm light source and an intensity of 100 mW/cm^2 in order to crosslink the PHC domains. We then performed atomic force microscopy (AFM) on sections of cured blends exhibiting

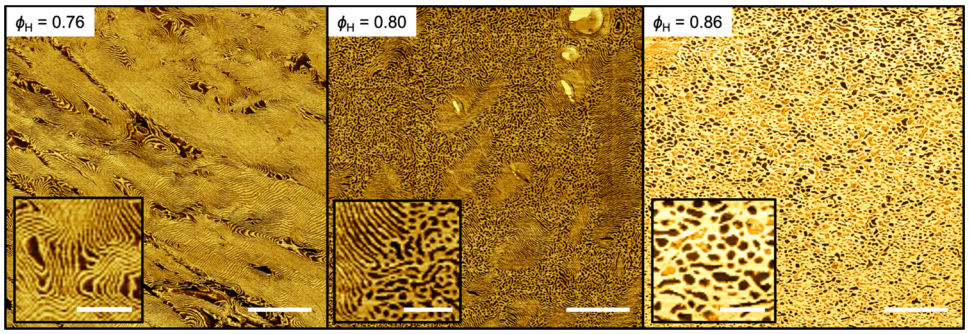

Figure 5. Atomic force microscopy phase images of the surfaces of blends cured at 70 °C exhibiting swollen LAM (ϕ_H = 0.76), coexisting LAM/BμE (ϕ_H = 0.80), and pure BμE (ϕ_H = 0.86). Scale bars = 2 μm (full-view) and 500 nm (inset).

https://doi.org/10.1021/acsami.2c22927
ACS Appl. Mater. Interfaces 2023, 15, 10044−10052

LAM (ϕ_H = 0.76), coexisting LAM/BμE (ϕ_H = 0.80), and BμE (ϕ_H = 0.86) morphologies according to SAXS. The substantial modulus difference between crosslinked PHC and uncrosslinked PM domains, provided good contrast in phase imaging and facilitated unambiguous structural characterization. The obtained AFM images strongly corroborate the SAXS data, with the expected morphology clearly present in each blend (Figure 5). As the homopolymer content increases from ϕ_H = 0.76 to ϕ_H = 0.80, highly swollen and fluctuating lamellae give way to coexistence where distinct micron-sized grains of well-ordered lamellae are embedded within a matrix of disordered BμE. It is also apparent that, at grain boundaries, lamellar layers smoothly transition to BμE with few defects. Notably, while BμE/LAM coexistence has been repeatedly found in A/B/AB ternary blends,[21,24,30,61] this work presents the first detailed image of the morphology in this system where both phases are unambiguously present, allowing elucidation of structural details that are not apparent in SAXS alone.

While the AFM images provide compelling evidence of co-continuity, AFM is inherently limited as a characterization tool by the difficulty of sample preparation, instrumental operation, and obtaining low-magnification images to assess the global morphology. Scanning electron microscopy (SEM) is a complementary imaging technique, as it can provide high-resolution images at nanometer-to-micron length scales with simpler sample preparation than AFM or transmission electron microscopy. However, the need to sputter-coat most polymeric samples means that phase contrast is lost in solid, non-porous materials. To address this problem, we leveraged the fact that the photocrosslinking chemistry is phase-selective, forming crosslinks within only a single domain, leaving an uncrosslinked homopolymer-rich phase that can be removed by solvent extraction. After extraction and drying, a nanoporous monolith remains in which the crosslinked domains are transcribed as topographical features, which are readily imaged by SEM.[37]

Fragments of cured blends were immersed in methanol to extract uncrosslinked PM domains, followed by solvent replacement with water and lyophilization to produce porous monoliths. SEM images of the monolith derived from the blend containing the 86% homopolymer unambiguously depict a structure consistent with the BμE (Figure 6). Highly fluctuating lamella-like sheets that interconnect into a continuous network structure are clearly present, complemented by a similarly continuous network of pores. Nearly perfect correspondence between this image and an AFM image obtained from the cured blend (Figure 5) indicates that solvent exposure did not disrupt the crosslinked morphology. Furthermore, low-magnification images (Figure S4) show a remarkably uniform network structure with few large-scale defects. No evidence of macrophase separation is observed in this sample, contradicting recent theory[35,36] that concluded that the BμE is unstable to phase separation into a 3-phase mixture. While the BμE could be sufficiently metastable to resist these annealing conditions (100 °C for 24 h)—a possibility alluded to by Matsen and colleagues—crosslinking obviates this concern for practical applications by covalently fixing the bicontinuous network structure.

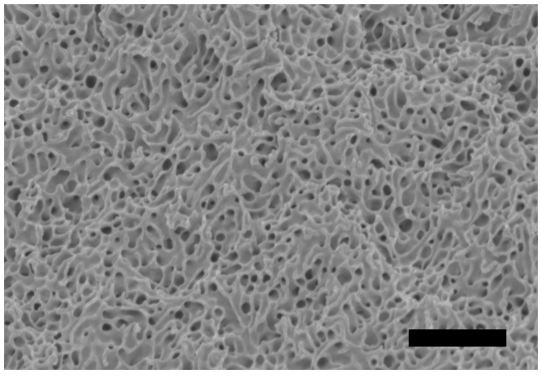

Figure 6. SEM image of the porous monolith prepared from a BμE (ϕ_H = 0.86). Scale bar = 1 μm.

Due to the ease of SEM sample preparation and operation, we next prepared and imaged porous monoliths from blends spanning the full compositional range across the BμE window (Figure 7). Remarkably, every phase observed in SAXS is apparent in this image library allowing for unprecedented insight into the morphological evolution of these materials as the composition is changed. Pure lamellae are evident up to ϕ_H = 0.76, at which point they are highly swollen and irregular, followed by BμE/LAM coexistence from ϕ_H = 0.78–0.80. Notably, the lamellar domains do not exhibit the same porosity as the BμE, likely due to collapse of adjacent lamellar sheets when the complementary PM-rich domains are removed. The large voids that are apparent in the ϕ_H = 0.60 and ϕ_H = 0.80 blends are likely due to exfoliation of lamellar layers during

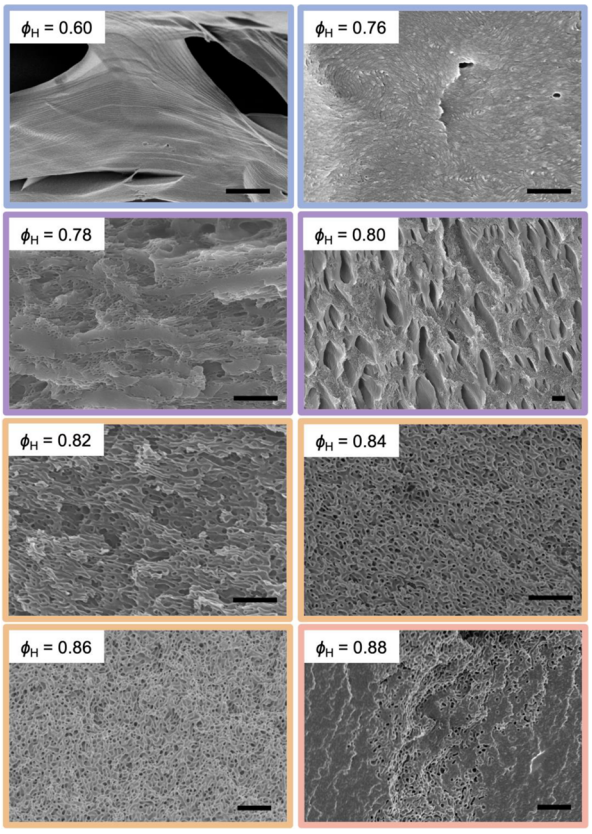

Figure 7. SEM images of voided crosslinked monoliths from blends cured at 70 °C, depicting morphological evolution from swollen LAM (ϕ_H = 0.60–0.76) to BμE/LAM coexistence (ϕ_H = 0.78–0.80) to pure BμE (ϕ_H = 0.82–0.86) to 3-phase coexistence (ϕ_H = 0.88). Border colors correspond to the phase diagram regions depicted in Figure 1. Scale bars = 1 μm.

https://doi.org/10.1021/acsami.2c22927
ACS Appl. Mater. Interfaces 2023, 15, 10044–10052

SEM sample preparation, as such features are not present in AFM images of cured blends (Figure 5). As the homopolymer content continues to approach the mean-field theory Lifshitz point, a pure BμE appears at ϕ_H = 0.82 and persists through ϕ_H = 0.86. At 0.88, 3-phase coexistence between macrophase-separated PM-rich, PHC-rich, and BμE regions appears, as evidenced by the presence of both large domains of the solid crosslinked polymer (Figure 7) and large voids (Figure S5).

Blend Photorheometry. In order to analyze how the blend microstructure can affect resultant physical properties, blends from ϕ_H = 0.60−0.88 were cured by irradiation with 365 nm light with an intensity of 100 mW/cm^2 at 70 °C while performing oscillatory shear rheometry to determine the effect of curing on mechanical properties. Similar to previous studies on LAM-forming diblock polymers,[49] the shear moduli strongly increased for all microphase-separated blends 5 min after the UV light was turned on (Figure S6). The catastrophic effect of macrophase separation on physical properties is evident by comparing the cure behavior of the ϕ_H = 0.86 (BμE) and ϕ_H = 0.88 (multiphase) blends (Figure 8).

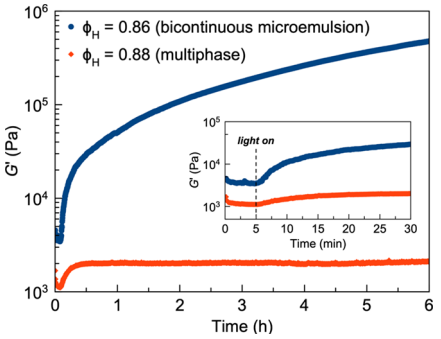

Figure 8. Photorheometry of polymer blends where ϕ_H = 0.86 with the microstructure assigned as BμE (blue trace) and where ϕ_H = 0.88 with the microstructure assigned as macrophase separation coexisting with BμE (orange trace). Temperature = 70 °C, strain = 0.5%, shear rate = 1.0 rad/s, and light intensity = 100 mW/cm^2.

Substantial stiffening occurred for the former due to the formation of a three-dimensionally percolating crosslinked network within the co-continuous BμE morphology. In the latter, however, the crosslinkable domains are largely localized within isolated PHC-rich droplets, which prevents the formation of an elastically effective network. This result highlights the importance of covalently crosslinking sensitive morphologies like the BμE if practical applications are intended—a compositional change of only 2% can cause complete annihilation of the desired material properties.

Ionic Conductivity. Solid polymer electrolytes have attracted substantial research interest due to their wide electrochemical stability window[65] and greater mechanical stabilization of electrode−electrolyte interfaces[66] compared to traditional liquid electrolytes, among other properties. Ordinarily, a tradeoff exists between good mechanical stability (which requires molecular rigidity) and high ion conductivity (which requires molecular mobility). Bicontinuous microphase-separated polymer materials have been found to bypass this inherent limitation due to the ability to separately engineer mechanically stiff and highly conductive domains.[4]

To demonstrate similar utility of crosslinked BμEs, we infiltrated the voids of a BμE-derived nanoporous monolith (blend ϕ_H = 0.84) with the ionic liquid 1-ethyl-3-methylimidazolium bis(trifluoromethylsulfonyl)imide ([C_2MIM][TFSI]). The strong polarity difference between the nonpolar crosslinked PHC domains and the ionic liquid implies that the conductive phase should be fully segregated from the supporting crosslinked network. Using AC impedance spectroscopy, a conductivity value of σ = 2.0 mS/cm was measured for the ionic liquid-filled material by taking the bulk resistance to be equal to the high-frequency plateau impedance (Z' = 87 Ω at the tan δ peak frequency) (Figure 9). Using a

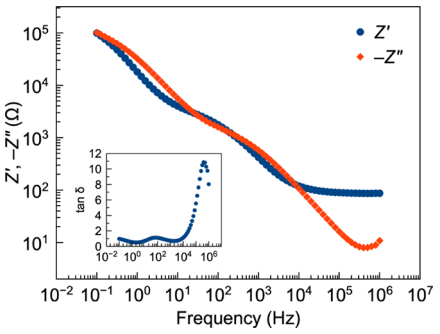

Figure 9. Bode plot of real (blue markers) and imaginary (orange markers) impedance as a function of AC frequency for the [C_2MIM][TFSI]-infiltrated monolith derived from the ϕ_H = 0.84 blend, with the inset depicting the loss tangent tan $\delta = Z''/Z'$.

literature conductivity for pure [C_2MIM][TFSI] = 8.2 mS/cm,[67] a "tortuosity factor" (τ) that describes the additional path length through which a charge must travel in a nonuniform, nonlinear electrolyte can be found:

$$\tau = \frac{\sigma_{IL}\phi_{IL}f}{\sigma_{SPE}} \quad (4)$$

where σ_{IL} is the conductivity of the pure ionic liquid, ϕ_{IL} is the volume fraction of the ionic liquid in the porous network, σ_{SPE} is the conductivity of the polymer electrolyte, and f is the morphology factor describing the three-dimensional connectivity in the idealized representation of the microstructure (f = 1 in co-continuous networks).[68,69] Assuming that only uncrosslinked PMEA homopolymer is extracted, the ionic liquid occupies a volume fraction of ϕ_{IL} = 0.42 and the resultant τ is calculated to be 1.8, indicating the presence of a highly uniform bicontinuous morphology. In terms of tortuosity, this BμE-based system slightly outperforms an ideal double gyroid network ($\tau \approx 2$)[68]—often considered a highly desirable morphology for microphase-separated solid polymer electrolytes.[70] These initial results indicate that crosslinked BμEs, in which one phase is insulating and mechanically robust while the other is an electrolyte, hold substantial promise as next-generation conductive materials. Here, we note that cooling the voided BμE material below the glass transition will result in a substantial increase in modulus by at least an order of magnitude (Tew and coworkers recorded a modulus of ca. 90 MPa for bicontinuous polystyrene/poly(ethylene oxide) crosslinked blends at 30 °C).[4] Accordingly, macroscopic parts can be formed in the rubbery state and then cooled below T_g, where the shape will be (reversibly) fixed.

CONCLUSIONS

Through phase-selective photocrosslinking, we have presented the most definitive characterization to date of BμE-forming

https://doi.org/10.1021/acsami.2c22927
ACS Appl. Mater. Interfaces 2023, 15, 10044−10052

polymer blends and established a basis for their further adaptation in advanced applications. The combination of SAXS, SEM, and AFM revealed that the BμE occupies a compositional range spanning nearly 10 vol % homopolymer—a remarkably wide and accessible window of phase space. The microstructural morphology profoundly directs emergent physical properties, as the substantial stiffening that occurs upon curing bicontinuous blends is entirely lost at the onset of macrophase separation. Finally, crosslinked BμEs were found to be promising materials for solid polymer electrolytes, with high conductivity values measured when the uncrosslinked continuous domain was filled with an ionic liquid.

One great advantage of BμEs compared to other co-continuous network phases is the simplicity of their preparation. Numerous different polymer chemistries, compositions, and molecular weights have been found to produce BμEs in A/B/AB ternary blends. Furthermore, as a thermodynamically stable state of soft matter, no specialized processes are needed to trap the co-continuous structure and prevent macroscopic coalescence. While further development is needed to facilitate the practical usage of polymeric BμEs, particularly with respect to achieving faster cure kinetics and photocrosslinking with commercially relevant polymers, we anticipate that this high degree of modularity will enable the design of co-continuous materials that can address a variety of contemporary challenges in material science.

■ ASSOCIATED CONTENT

Supporting Information

The Supporting Information is available free of charge at https://pubs.acs.org/doi/10.1021/acsami.2c22927.

Instrumental details, experimental procedures, supplementary figures, and molecular characterization data (PDF)

■ AUTHOR INFORMATION

Corresponding Authors

Timothy P. Lodge − *Department of Chemical Engineering and Materials Science and Department of Chemistry, University of Minnesota, Minneapolis, Minnesota 55455, United States;* orcid.org/0000-0001-5916-8834; Email: lodge@umn.edu

Frank S. Bates − *Department of Chemical Engineering and Materials Science, University of Minnesota, Minneapolis, Minnesota 55455, United States;* orcid.org/0000-0003-3977-1278; Email: bates001@umn.edu

Authors

Michael B. Sims − *Department of Chemical Engineering and Materials Science, University of Minnesota, Minneapolis, Minnesota 55455, United States;* orcid.org/0000-0002-5308-3386

Joshua W. Goetze − *Department of Chemical Engineering and Materials Science, University of Minnesota, Minneapolis, Minnesota 55455, United States*

Gabriela Diaz Gorbea − *Department of Chemical Engineering and Materials Science, University of Minnesota, Minneapolis, Minnesota 55455, United States*

Zachary M. Gdowski − *Department of Chemical Engineering and Materials Science, University of Minnesota, Minneapolis, Minnesota 55455, United States*

Complete contact information is available at: https://pubs.acs.org/10.1021/acsami.2c22927

Notes

The authors declare no competing financial interest.

■ ACKNOWLEDGMENTS

This work was supported by the Office of Basic Energy Sciences (BES) of the U.S. Department of Energy (DoE) under Contract DE-SC0017809. SAXS, SEM, and AFM were carried out in the Characterization Facility, University of Minnesota, which receives partial support from the National Science Foundation MRSEC (DMR-2011401) and NNCI (ECCS-2025124) programs. Joanna White and Stephanie Liffland are gratefully acknowledged for their assistance in performing synchrotron X-ray scattering experiments.

■ REFERENCES

(1) Register, R. A. Continuity through Dispersity. *Nature* **2012**, *483*, 167−168.

(2) Hsu, W. Y.; Wu, S. Percolation Behavior in Morphology and Modulus of Polymer Blends. *Polym. Eng. Sci.* **1993**, *33*, 293−302.

(3) Cirkel, P. A.; Okada, T. A Comparison of Mechanical and Electrical Percolation During the Gelling of Nafion Solutions. *Macromolecules* **2000**, *33*, 4921−4925.

(4) Walker, C. N.; Bryson, K. C.; Hayward, R. C.; Tew, G. N. Wide Bicontinuous Compositional Windows from Co-Networks Made with Telechelic Macromonomers. *ACS Nano* **2014**, *8*, 12376−12385.

(5) Burban, J. H.; He, M.; Cussler, E. L. Organic Microporous Materials Made by Bicontinuous Microemulsion Polymerization. *AIChE J.* **1995**, *41*, 907−914.

(6) Jones, B. H.; Lodge, T. P. High-Temperature Nanoporous Ceramic Monolith Prepared from a Polymeric Bicontinuous Microemulsion Template. *J. Am. Chem. Soc.* **2009**, *131*, 1676−1677.

(7) Jones, B. H.; Lodge, T. P. Nanoporous Materials Derived from Polymeric Bicontinuous Microemulsions. *Chem. Mater.* **2010**, *22*, 1279−1281.

(8) Seo, M.; Hillmyer, M. A. Reticulated Nanoporous Polymers by Controlled Polymerization-Induced Microphase Separation. *Science* **2012**, *336*, 1422−1425.

(9) Hsueh, H.-Y.; Yao, C.-T.; Ho, R.-M. Well-Ordered Nanohybrids and Nanoporous Materials from Gyroid Block Copolymer Templates. *Chem. Soc. Rev.* **2015**, *44*, 1974−2018.

(10) du Fresne von Hohenesche, C.; Schmidt, D. F.; Schädler, V. Nanoporous Melamine−Formaldehyde Gels by Microemulsion Templating. *Chem. Mater.* **2008**, *20*, 6124−6129.

(11) Desai, S. D.; Gordon, R. D.; Gronda, A. M.; Cussler, E. L. Polymerized Microemulsions. *Curr. Opin. Colloid Interface Sci.* **1996**, *1*, 519−522.

(12) Bates, F. S.; Maurer, W. W.; Lipic, P. M.; Hillmyer, M. A.; Almdal, K.; Mortensen, K.; Fredrickson, G. H.; Lodge, T. P. Polymeric Bicontinuous Microemulsions. *Phys. Rev. Lett.* **1997**, *79*, 849−852.

(13) Chen, S. H.; Chang, S. L.; Strey, R.; Samseth, J.; Mortensen, K. Structural Evolution of Bicontinuous Microemulsions. *J. Phys. Chem.* **1991**, *95*, 7427−7432.

(14) Sakurai, S.; Iwane, K.; Nomura, S. Morphology of Poly(styrene-*block*-butadiene-*block*-styrene) Triblock Copolymers Crosslinked in the Disordered State. *Macromolecules* **1993**, *26*, 5479−5486.

(15) Li, L.; Shen, X.; Hong, S. W.; Hayward, R. C.; Russell, T. P. Fabrication of Co-Continuous Nanostructured and Porous Polymer Membranes: Spinodal Decomposition of Homopolymer and Random Copolymer Blends. *Angew. Chem., Int. Ed.* **2012**, *51*, 4089−4094.

(16) Bryson, K. C.; Löbling, T. I.; Müller, A. H. E.; Russell, T. P.; Hayward, R. C. Using Janus Nanoparticles to Trap Polymer Blend Morphologies During Solvent-Evaporation-Induced Demixing. *Macromolecules* **2015**, *48*, 4220−4227.

(17) Zeng, D.; Ribbe, A.; Hayward, R. C. Anisotropic and Interconnected Nanoporous Materials from Randomly End-Linked Copolymer Networks. *Macromolecules* **2017**, *50*, 4668−4676.
(18) Tran-Cong-Miyata, Q.; Nishigami, S.; Ito, T.; Komatsu, S.; Norisuye, T. Controlling the Morphology of Polymer Blends Using Periodic Irradiation. *Nat. Mater.* **2004**, *3*, 448−451.
(19) Shim, J.; Bates, F. S.; Lodge, T. P. Bicontinuous Microemulsions in Partially Charged Ternary Polymer Blends. *ACS Macro Lett.* **2019**, *8*, 1166−1171.
(20) Shim, J.; Xie, S.; Bates, F. S.; Lodge, T. P. Effect of Ion Concentration on the Formation of Bicontinuous Microemulsions in Partially Charged Ternary Polymer Blends. *Macromolecules* **2019**, *52*, 9416−9424.
(21) Zheng, C.; Zhang, B.; Bates, F. S.; Lodge, T. P. Self-Assembly of Partially Charged Diblock Copolymer-Homopolymer Ternary Blends. *Macromolecules* **2022**, *55*, 4766−4775.
(22) Jeon, H. S.; Lee, J. H.; Balsara, N. P.; Newstein, M. C. An Experimental Study of the Thermodynamic Properties of Multicomponent Polyolefin Blends with Ordered and Disordered Phases. *Macromolecules* **1998**, *31*, 3340−3352.
(23) Corvazier, L.; Messé, L.; Salou, C. L. O.; Young, R. N.; Fairclough, J. P. A.; Ryan, A. J. Lamellar Phases and Microemulsions in Model Ternary Blends Containing Amphiphilic Block Copolymers. *J. Mater. Chem.* **2001**, *11*, 2864−2874.
(24) Messé, L. C.; Corvazier, L.; Ryan, A. J. Effect of the Molecular Weight of the Homopolymers on the Morphology in Ternary Blends of Polystyrene, Polyisoprene, Polystyrene-*block*-Polyisoprene Copolymer. *Polymer* **2003**, *44*, 7397−7403.
(25) Reynolds, B. J.; Ruegg, M. L.; Balsara, N. P.; Radke, C. J.; Shaffer, T. D.; Lin, M. Y.; Shull, K. R.; Lohse, D. J. Thermodynamics of Polymer Blends Organized by Balanced Block Copolymer Surfactants Studied by Mean-Field Theories and Scattering. *Macromolecules* **2004**, *37*, 7401−7417.
(26) Habersberger, B. M.; Bates, F. S.; Lodge, T. P. Hierarchical Microphase Separation in Bicontinuous Ternary Polymer Blends. *Soft Matter* **2012**, *8*, 3429−3441.
(27) Habersberger, B. M.; Gillard, T. M.; Hickey, R. J.; Lodge, T. P.; Bates, F. S. Fluctuation Effects in Symmetric Diblock Copolymer−Homopolymer Ternary Mixtures near the Lamellar−Disorder Transition. *ACS Macro Lett.* **2014**, *3*, 1041−1045.
(28) Hickey, R. J.; Gillard, T. M.; Irwin, M. T.; Lodge, T. P.; Bates, F. S. Structure, Viscoelasticity, and Interfacial Dynamics of a Model Polymeric Bicontinuous Microemulsion. *Soft Matter* **2016**, *12*, 53−66.
(29) Hickey, R. J.; Gillard, T. M.; Irwin, M. T.; Morse, D. C.; Lodge, T. P.; Bates, F. S. Phase Behavior of Diblock Copolymer−Homopolymer Ternary Blends: Congruent First-Order Lamellar−Disorder Transition. *Macromolecules* **2016**, *49*, 7928−7944.
(30) Irwin, M. T.; Hickey, R. J.; Xie, S.; Bates, F. S.; Lodge, T. P. Lithium Salt-Induced Microstructure and Ordering in Diblock Copolymer/Homopolymer Blends. *Macromolecules* **2016**, *49*, 4839−4849.
(31) Xie, S.; Meyer, D. J.; Wang, E.; Bates, F. S.; Lodge, T. P. Structure and Properties of Bicontinuous Microemulsions from Salt-Doped Ternary Polymer Blends. *Macromolecules* **2019**, *52*, 9693−9702.
(32) Xie, S.; Zhang, B.; Bates, F. S.; Lodge, T. P. Phase Behavior of Salt-Doped A/B/AB Ternary Polymer Blends: The Role of Homopolymer Distribution. *Macromolecules* **2021**, *54*, 6990−7002.
(33) Ellison, C. J.; Meuler, A. J.; Qin, J.; Evans, C. M.; Wolf, L. M.; Bates, F. S. Bicontinuous Polymeric Microemulsions from Polydisperse Diblock Copolymers. *J. Phys. Chem. B* **2009**, *113*, 3726−3737.
(34) Jones, B. H.; Lodge, T. P. Hierarchically Structured Materials from Block Polymer Confinement within Bicontinuous Microemulsion-Derived Nanoporous Polyethylene. *ACS Nano* **2011**, *5*, 8914−8927.
(35) Vorselaars, B.; Spencer, R. K. W.; Matsen, M. W. Instability of the Microemulsion Channel in Block Copolymer-Homopolymer Blends. *Phys. Rev. Lett.* **2020**, *125*, No. 117801.
(36) Spencer, R. K. W.; Matsen, M. W. Coexistence of Polymeric Microemulsion with Homopolymer-Rich Phases. *Macromolecules* **2021**, *54*, 1329−1337.
(37) Zhou, N.; Bates, F. S.; Lodge, T. P. Mesoporous Membrane Templated by a Polymeric Bicontinuous Microemulsion. *Nano Lett.* **2006**, *6*, 2354−2357.
(38) Chen, Y.; Chou, C.-F. Reversible Photodimerization of Coumarin Derivatives Dispersed in Poly(Vinyl Acetate). *J. Polym. Sci., Part A: Polym. Chem.* **1995**, *33*, 2705−2714.
(39) Jiang, J.; Qi, B.; Lepage, M.; Zhao, Y. Polymer Micelles Stabilization on Demand through Reversible Photo-Cross-Linking. *Macromolecules* **2007**, *40*, 790−792.
(40) Nagata, M.; Yamamoto, Y. Photoreversible Poly(ethylene glycol)s with Pendent Coumarin Group and Their Hydrogels. *React. Funct. Polym.* **2008**, *68*, 915−921.
(41) He, J.; Tremblay, L.; Lacelle, S.; Zhao, Y. Preparation of Polymer Single Chain Nanoparticles Using Intramolecular Photodimerization of Coumarin. *Soft Matter* **2011**, *7*, 2380−2386.
(42) He, J.; Zhao, Y. Light-Responsive Polymer Micelles, Nano- and Microgels Based on the Reversible Photodimerization of Coumarin. *Dyes Pigm.* **2011**, *89*, 278−283.
(43) Azagarsamy, M. A.; McKinnon, D. D.; Alge, D. L.; Anseth, K. S. Coumarin-Based Photodegradable Hydrogel: Design, Synthesis, Gelation, and Degradation Kinetics. *ACS Macro Lett.* **2014**, *3*, 515−519.
(44) Kabb, C. P.; O'Bryan, C. S.; Deng, C. C.; Angelini, T. E.; Sumerlin, B. S. Photoreversible Covalent Hydrogels for Soft-Matter Additive Manufacturing. *ACS Appl. Mater. Interfaces* **2018**, *10*, 16793−16801.
(45) Zhu, C. N.; Li, C. Y.; Wang, H.; Hong, W.; Huang, F.; Zheng, Q.; Wu, Z. L. Reconstructable Gradient Structures and Reprogrammable 3D Deformations of Hydrogels with Coumarin Units as the Photolabile Crosslinks. *Adv. Mater.* **2021**, *33*, No. 2008057.
(46) Maddipatla, M. V. S. N.; Wehrung, D.; Tang, C.; Fan, W.; Oyewumi, M. O.; Miyoshi, T.; Joy, A. Photoresponsive Coumarin Polyesters That Exhibit Cross-Linking and Chain Scission Properties. *Macromolecules* **2013**, *46*, 5133−5140.
(47) Govindarajan, S. R.; Xu, Y.; Swanson, J. P.; Jain, T.; Lu, Y.; Choi, J.-W.; Joy, A. A Solvent and Initiator Free, Low-Modulus, Degradable Polyester Platform with Modular Functionality for Ambient-Temperature 3D Printing. *Macromolecules* **2016**, *49*, 2429−2437.
(48) Defize, T.; Thomassin, J.-M.; Ottevaere, H.; Malherbe, C.; Eppe, G.; Jellali, R.; Alexandre, M.; Jérôme, C.; Riva, R. Photo-Cross-Linkable Coumarin-Based Poly(ε-Caprolactone) for Light-Controlled Design and Reconfiguration of Shape-Memory Polymer Networks. *Macromolecules* **2019**, *52*, 444−456.
(49) Sims, M. B.; Zhang, B.; Gdowski, Z. M.; Lodge, T. P.; Bates, F. S. Nondestructive Photo-Cross-Linking of Microphase-Separated Diblock Polymers through Coumarin Dimerization. *Macromolecules* **2022**, *55*, 3317−3324.
(50) Tietz, K.; Finkhäuser, S.; Samwer, K.; Vana, P. Stabilizing the Microphase Separation of Block Copolymers by Controlled Photo-Crosslinking. *Macromol. Chem. Phys.* **2014**, *215*, 1563−1572.
(51) Child, W. C.; Ferry, J. D. Dynamic Mechanical Properties of Poly-*n*-Hexyl Methacrylate. *J. Colloid Sci.* **1957**, *12*, 389−399.
(52) Shipp, D. A.; Wang, J.-L.; Matyjaszewski, K. Synthesis of Acrylate and Methacrylate Block Copolymers Using Atom Transfer Radical Polymerization. *Macromolecules* **1998**, *31*, 8005−8008.
(53) Anastasaki, A.; Waldron, C.; Wilson, P.; Boyer, C.; Zetterlund, P. B.; Whittaker, M. R.; Haddleton, D. High Molecular Weight Block Copolymers by Sequential Monomer Addition Via Cu(0)-Mediated Living Radical Polymerization (SET-LRP): An Optimized Approach. *ACS Macro Lett.* **2013**, *2*, 896−900.
(54) Broseta, D.; Fredrickson, G. H. Phase Equilibria in Copolymer/Homopolymer Ternary Blends: Molecular Weight Effects. *J. Chem. Phys.* **1990**, *93*, 2927−2938.
(55) Van Krevelen, D. W.; Hoftyzer, P. J. Prediction of Polymer Densities. *J. Appl. Polym. Sci.* **1969**, *13*, 871−881.

https://doi.org/10.1021/acsami.2c22927
ACS Appl. Mater. Interfaces 2023, 15, 10044−10052

(56) Hashimoto, T.; Tanaka, H.; Hasegawa, H. Ordered Structure in Mixtures of a Block Copolymer and Homopolymers. 2. Effects of Molecular Weights of Homopolymers. *Macromolecules* **1990**, *23*, 4378−4386.
(57) Düchs, D.; Ganesan, V.; Fredrickson, G. H.; Schmid, F. Fluctuation Effects in Ternary AB + A + B Polymeric Emulsions. *Macromolecules* **2003**, *36*, 9237−9248.
(58) Matsen, M. W. Phase Behavior of Block Copolymer/Homopolymer Blends. *Macromolecules* **1995**, *28*, 5765−5773.
(59) Bates, F. S.; Maurer, W.; Lodge, T. P.; Schulz, M. F.; Matsen, M. W.; Almdal, K.; Mortensen, K. Isotropic Lifshitz Behavior in Block Copolymer-Homopolymer Blends. *Phys. Rev. Lett.* **1995**, *75*, 4429−4432.
(60) Morales, D.; Gutiérrez, J. M.; García-Celma, M. J.; Solans, Y. C. A Study of the Relation between Bicontinuous Microemulsions and Oil/Water Nano-Emulsion Formation. *Langmuir* **2003**, *19*, 7196−7200.
(61) Washburn, N. R.; Lodge, T. P.; Bates, F. S. Ternary Polymer Blends as Model Surfactant Systems. *J. Phys. Chem. B* **2000**, *104*, 6987−6997.
(62) Tanaka, H.; Hasegawa, H.; Hashimoto, T. Ordered Structure in Mixtures of a Block Copolymer and Homopolymers. 1. Solubilization of Low Molecular Weight Homopolymers. *Macromolecules* **1991**, *24*, 240−251.
(63) Teubner, M.; Strey, R. Origin of the Scattering Peak in Microemulsions. *J. Chem. Phys.* **1987**, *87*, 3195−3200.
(64) Morkved, T. L.; Stepanek, P.; Krishnan, K.; Bates, F. S.; Lodge, T. P. Static and Dynamic Scattering from Ternary Polymer Blends: Bicontinuous Microemulsions, Lifshitz Lines, and Amphiphilicity. *J. Chem. Phys.* **2001**, *114*, 7247−7259.
(65) Marchiori, C. F. N.; Carvalho, R. P.; Ebadi, M.; Brandell, D.; Araujo, C. M. Understanding the Electrochemical Stability Window of Polymer Electrolytes in Solid-State Batteries from Atomic-Scale Modeling: The Role of Li-Ion Salts. *Chem. Mater.* **2020**, *32*, 7237−7246.
(66) Khurana, R.; Schaefer, J. L.; Archer, L. A.; Coates, G. W. Suppression of Lithium Dendrite Growth Using Cross-Linked Polyethylene/Poly(ethylene oxide) Electrolytes: A New Approach for Practical Lithium-Metal Polymer Batteries. *J. Am. Chem. Soc.* **2014**, *136*, 7395−7402.
(67) Gouverneur, M.; Schmidt, F.; Schönhoff, M. Negative Effective Li Transference Numbers in Li Salt/Ionic Liquid Mixtures: Does Li Drift in the "Wrong" Direction? *Phys. Chem. Chem. Phys.* **2018**, *20*, 7470−7478.
(68) Hallinan, D. T.; Balsara, N. P. Polymer Electrolytes. *Annu. Rev. Mater. Res.* **2013**, *43*, 503−525.
(69) Hallinan, D. T.; Villaluenga, I.; Balsara, N. P. Polymer and Composite Electrolytes. *MRS Bull.* **2018**, *43*, 759−767.
(70) Jo, G.; Ahn, H.; Park, M. J. Simple Route for Tuning the Morphology and Conductivity of Polymer Electrolytes: One End Functional Group Is Enough. *ACS Macro Lett.* **2013**, *2*, 990−995.

https://doi.org/10.1021/acsami.2c22927
ACS Appl. Mater. Interfaces 2023, 15, 10044−10052